Sulfur-Infiltrated Graphene-Based Layered Porous Carbon Cathodes for High-Performance Lithium–Sulfur Batteries

Xi Yang, Long Zhang, Fan Zhang, Yi Huang, and Yongsheng Chen*

Key Laboratory of Functional Polymer Materials, Collaborative Innovation Center of Chemical Science and Engineering (Tianjin), Center for Nanoscale Science and Technology, Institute of Polymer Chemistry, College of Chemistry, Nankai University, Tianjin 300071, China

ABSTRACT Because of advantages such as excellent electronic conductivity, high theoretical specific surface area, and good mechanical flexibility, graphene is receiving increasing attention as an additive to improve the conductivity of sulfur cathodes in lithium–sulfur (Li–S) batteries. However, graphene is not an effective substrate material to confine the polysulfides in cathodes and stable the cycling. Here, we designed and synthesized a graphene-based layered porous carbon material for the impregnation of sulfur as cathode for Li–S battery. In this composite, a thin layer of porous carbon uniformly covers both surfaces of the graphene and sulfur is highly dispersed in its pores. The high specific surface area and pore volume of the porous carbon layers not only can achieve a high sulfur loading in highly dispersed amorphous state, but also can act as polysulfide reservoirs to alleviate the shuttle effect. When used as the cathode material in Li–S batteries, with the help of the thin porous carbon layers, the as-prepared materials demonstrate a better electrochemical performance and cycle stability compared with those of graphene/sulfur composites.

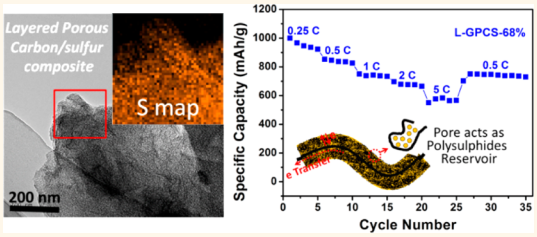

KEYWORDS: graphene · layered porous carbon · infiltrated · sulfur cathode · lithium–sulfur battery

Energy storage systems, with low cost, high energy density, and long cycle life, are crucial for the extensive deployment of portable electronic devices, electric vehicles, and for renewable energy applications.[1−3] Among the various types of rechargeable batteries, lithium–sulfur (Li–S) batteries have attracted great interest due to their high theoretical specific energy of 2600 Wh kg^{-1}, which is based on the assumption of the complete reaction of Li with S to form Li_2S.[1,4] However, commercial applications of Li–S batteries have not been very successful, despite significant progress having been made.[5−16] Two major challenges still remain for Li–S batteries: (1) The poor electronic conductivity of sulfur and the discharge products (Li_2S/Li_2S_2) leads to the low utilization of sulfur cathodes and limits the rate capability of Li–S batteries; (2) the polysulfides formed during discharge/charge cycles are highly soluble and can diffuse outside the cathode where they are then reduced to solid precipitates in the form of Li_2S or Li_2S_2 on the anode (Shuttle effect),[17] leading to the loss of active cathodic material and poor cycling performance.

To improve the electrical conductivity of the sulfur cathodes and to confine the polysulfides in the cathodes, various sulfur-based composites have been fabricated such as carbon–sulfur composites,[5,6,14,18−20] polymer-sulfur composites,[8,21−23] carbon-polymer-sulfur composites[24,25] and metal oxide-sulfur composites.[13] Among the available matrix materials, graphene, a single-atom-thick two-dimensional layer of carbon atoms with high theoretical surface area, superior electrical conductivity, and mechanical flexibility, has opened new possibilities and has been successfully used in Li–S batteries.[16,26−32] The high specific surface area (SSA) can achieve a high sulfur loading; the superior electronic conductivity can facilitate electron transport not only across the sulfur, but also in cathodes without the addition of any conducting filler. However, graphene is not an effective matrix material to confine the polysulfides in cathodes

* Address correspondence to yschen99@nankai.edu.cn.

Received for review March 5, 2014 and accepted April 21, 2014.

Published online April 21, 2014
10.1021/nn501284q

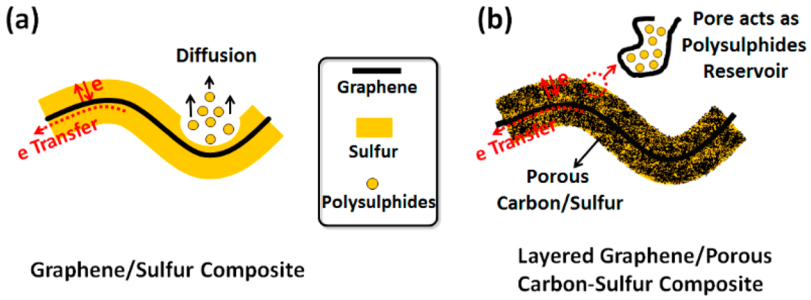

Figure 1. (a) The schematic architecture of the graphene/sulfur composite. Graphene acts both as a substrate to disperse the sulfur and an electronic conductive channel. However, polysulfides can readily diffuse outside the cathode. (b) The schematic architecture of the layered graphene/porous carbon−sulfur composite, proposed in this work. An extra thin layer of porous carbon uniformly covers both surfaces of the graphene, and sulfur is highly dispersed in its pores. The porous carbon acts as a polysulfide reservoir to alleviate the shuttle effect.

during the discharge/charge processes. Polysulfides can still readily diffuse outside the cathodes and initiate the "shuttle" problem, which significantly undermines the cycling performance (Figure 1a). To alleviate the "shuttle" problem, graphene oxide with oxygen functional groups has been used as an alternative to graphene to improve the cycling stability.[16,29] Furthermore, some polymers have also been used to wrap the graphene/sulfur composites and construct a three-dimensional network to prevent the diffusion of polysulfides.[33,34] However, the functionalization and addition of polymers usually will lower electron transport in the cathodes and excess conducting filler must be added to increase the conductivity, which further reduces the sulfur loading in the cathodes. Therefore, it remains challenging to design a new structure for graphene/sulfur composites, not merely to ensure a high sulfur loading and excellent electronic conductivity, but also to confine the polysulfides in the cathodes.

Herein, we present the rational design and synthesis of a graphene-based layered structure (Figure 1b) for the impregnation of sulfur as cathode for Li−S battery. A thin layer of porous carbon uniformly covers both surfaces of the graphene, and sulfur is highly dispersed in its pores. In this architecture, graphene acts as the electronic conductive channel and porous carbon acts as a polysulfide reservoir to alleviate the shuttle effect. Furthermore, the high SSA and pore volume of the porous carbon layers can simultaneously achieve a high sulfur loading and high sulfur utilization. When used as the cathode material in Li−S batteries, the as-prepared materials demonstrate a better electrochemical performance and cycle stability compared with those of graphene/sulfur composites.

RESULTS AND DISCUSSION

The layered graphene-based porous carbon (L-GPC) material was experimentally realized through hydrothermal and chemical activation processes as shown schematically in Figure 2a (Experimental Section). Phenolic resin (PR) was chosen as the precursor of porous carbon, because it has been widely used for preparation of activated carbon by chemical activation. More importantly, because of the $\pi-\pi$ interaction of phenol and graphene oxide (GO), the PR will only polymerized on the surfaces of GO in the hydrothermal polymerization process, and not elsewhere. Scanning electron microscopy (SEM) images of the morphology of GO/PR composites are shown in Figure 2b and Figure S1. A thin layer of PR is uniformly covered on both surfaces of the GO without bulk PR observed, and the layered GO/PR composites are interconnected and overlap to form a 3D porous foam structure. The 3D GO/PR was then chemically activated by KOH to obtain the final L-GPC material.[35] In this process, the PR was activated to form porous carbon and GO was reduced to graphene. The SEM image of the structure of L-GPC in Figure 2c clearly shows a layered, crumpled graphene-like structure. Transmission electron microscopy (TEM) images reveal the L-GPC material in details. As shown in Figure 2d,e, a thin layer of porous carbon uniformly covers both surfaces of the graphene sheet. The microstructure of the porous carbon covering the graphene sheets, was further studied at higher magnifications (Figure 2f) and reveals abundant pores surrounded by highly curved nanographene fragments. The short, linear features could be identified as individual nanographene fragments viewed edge-on.[36] Furthermore, the porosity of L-GPC was characterized by nitrogen (77.4 K) adsorption/desorption experiments and the isotherm is shown in Figure 2g. L-GPC has both a very high nitrogen BET SSA of up to 2500 m^2 g^{-1} and a very large pore volume of 1.937 cm^3 g^{-1}, which can ensure a high sulfur loading without reducing the electronic conductivity of sulfur. Pore size distribution analysis was performed using the nitrogen adsorption data by applying a nonlocal density functional theory (NL-DFT) kernel for the micromesopore size distribution, assuming a slit pore geometry for micro and mesopores. The analysis reveals the presence of micro-mesopores in the 1−10 nm size range, which can act as polysulfide reservoirs to alleviate the shuttle effect.

Layered graphene/porous carbon−sulfur (L-GPCS) composite was prepared using liquid-phase infiltration

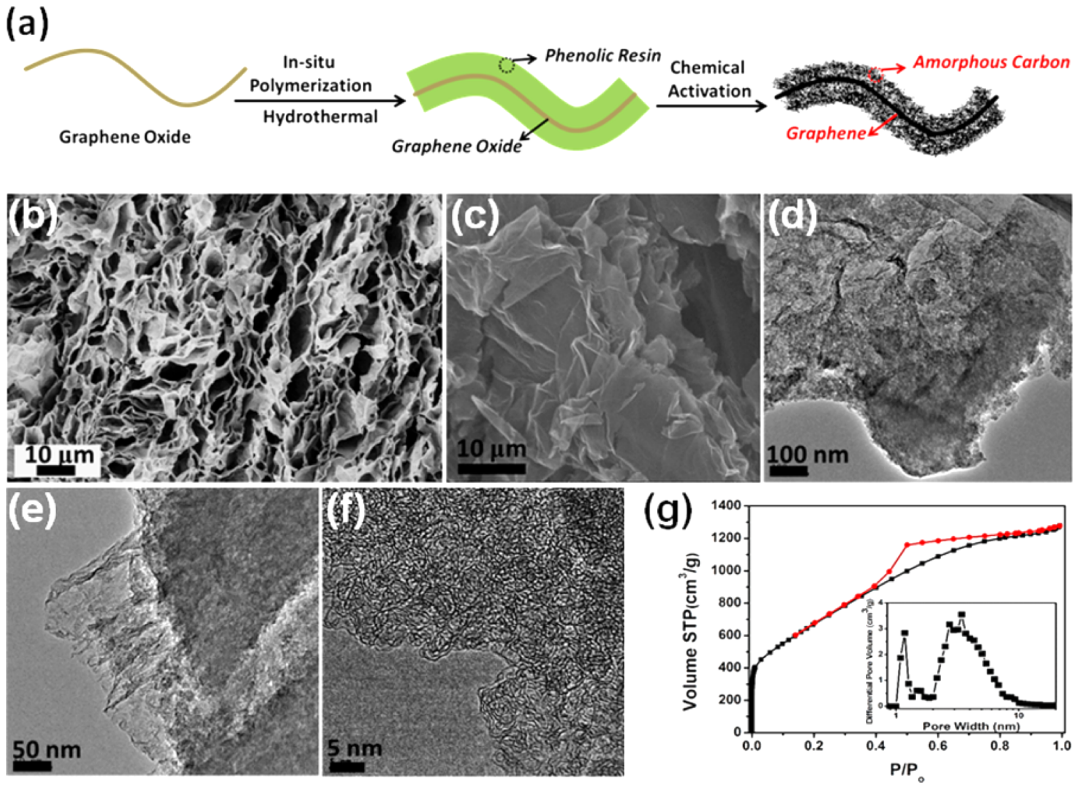

Figure 2. (a) A schematic showing the preparation of L-GPC material. (b) SEM image of the structure of the 3D GO/PR intermediate product. Structural characterization of L-GPC material: (c) SEM, (d−f) TEM. (g) Pore characterization of the L-GPC material.

and melt diffusion processes (Experimental Section). In L-GPCS composite, the sulfur homogeneously dispersed in the pores of porous carbon without bulk sulfur was observed from the TEM image (Figure 3a), scanning transmission electron microscopy (STEM) image (Figure 3b), and the corresponding elemental mapping of sulfur (Figure 3c). The existence of sulfur in L-GPCS composite was further confirmed by X-ray photoelectron spectroscopy (XPS) analysis, shown in Figure S2. The content of sulfur in L-GPCS composite was determined through thermogravimetric analysis (TGA) in nitrogen. As shown in Figure 3c, the TGA analyses indicate that the sulfur loading in the L-GPCS is 68 wt % (denoted as L-GPCS-68%). In addition, the sulfur in L-GPCS is more thermally stable than in the pure state, indicating the strong adsorption of the pores of the L-GPC matrix, which could alleviate the diffusion of polysulfides.[20] X-ray diffraction (XRD) patterns of the pure sulfur powder, L-GPCS-68%, and L-GPC are presented in Figure 3e. Usually, sulfur exists in a crystalline state with an orthorhombic structure at room temperature. After impregnation into the L-GPC matrix, the diffraction peaks disappeared, demonstrating that the sulfur existed in a highly dispersed amorphous state,[37] which could result in the high utilization of sulfur in electrochemical reactions. Furthermore, the L-GPC matrix shows a very weak and extremely broad (002) peak in the 15°−30° range caused by the amorphous porous carbon covering the graphene sheets.[35] Raman spectroscopy was used to further investigate the structural features of pure sulfur powder, L-GPCS-68%, and L-GPC (Figure 3f). The Raman spectra of L-GPC exhibits two broad and overlapping peaks with intensity maxima at ∼1350 cm^{-1} (D band) and at ∼1585 cm^{-1} (G band), which can be assigned to defects and sp^2 carbon networks in the L-GPC matrix, respectively.[38] Meanwhile, the sulfur powder exhibits characteristic peaks in the range 100−500 cm^{-1}, which are related to vibration of the S−S bond in S_8 species.[7] However, the sulfur-impregnated L-GPCS-68% did not show noticeable characteristic sulfur peaks, indicating S_8 molecules loading in L-GPC matrix without long-range ordering, similar to single molecule dispersion, which is consistent with the conclusion from XRD spectra.

The electrochemical performance of the L-GPCS-68% material as the cathode of a Li−S battery was evaluated with CR2032 coin cell. The cathode was fabricated without any addition of conducting filler, and contains 90 wt % L-GPCS-68% material and 10 wt % PVDF as binder, accounting for ∼62 wt % of sulfur in the cathode, with a typical sulfur mass loading of 0.65−0.75 mg cm^{-2}. The electrolyte used was 1.0 M lithium bis-trifluoromethanesulfonylimide (LiTFSI) in a mixed solvent of 1,3-dioxolane and 1,2-dimethoxyethane (1:1, v/v), with $LiNO_3$ (2 wt %) as an additive to

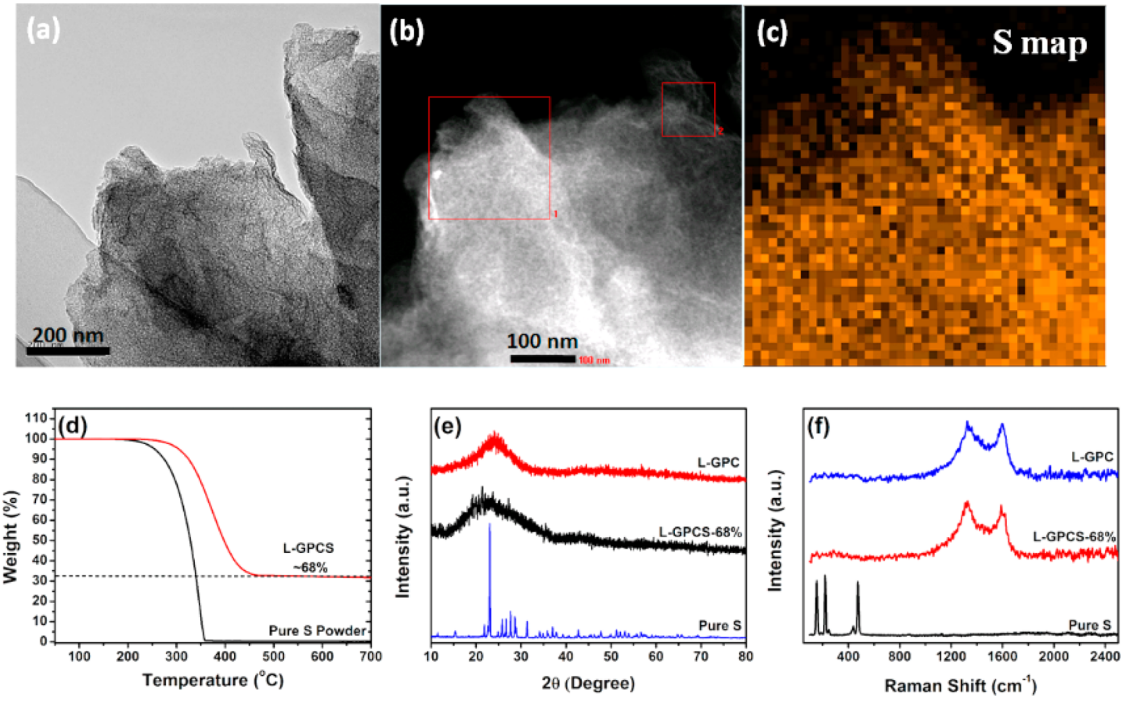

Figure 3. (a) TEM image of L-GPCS. (b) STEM image of L-GPCS in dark field. (c) Elemental mapping of the region shown in the red square 1 of (b) for sulfur reveals a homogeneous sulfur loading in the layered porous carbon. (d) Thermogravimetric curves of pure sulfur powder and the prepared L-GPCS material in N_2 with a heating rate of 10 K min^{-1}, indicating a sulfur content of 68 wt % in L-GPCS material. (e) XRD patterns of the pure sulfur powder, L-GPCS-68% and L-GPC. (f) Raman spectra of pure sulfur powder, L-GPCS-68%, and L-GPC. The XRD patterns and Raman spectra demonstrate that the sulfur existed in a highly dispersed amorphous state.

help passivate the surface of the lithium anode and reduce the shuttle effect.[39]

Cyclic voltammetry (CV) was used to reveal the electrochemical reaction mechanism of the L-GPCS-68% cathode measured between 1.5 and 3 V at a sweep rate of 0.1 mV s^{-1} for the first, second, and third cycles, as shown in Figure 4a. Two cathodic peaks are observed due to the multiple reduction of sulfur in the presence of Li ions. For the first cycle, the peak at ~2.25 V is related to the open ring reduction of the cyclic S_8 to long chain lithium polysulfides (Li_2S_x, $4 < x < 8$). The peak in the region of ~2 V is associated with further reduction of these polysulfides to Li_2S_2 and Li_2S. These two changes correspond to the two discharge plateaus in the discharge curve. An anodic peak at ~2.45 V can be attributed to the oxidation of Li_2S and Li_2S_2 to Li_2S_8 and a complete reverse reaction to sulfur does not take place.[40] From the second cycle, both the CV peak positions and areas remain almost unchanged, suggesting relatively good capacity retention.

The rate capability of the L-GPCS-68% cathode is measured at different current rates of 0.25, 0.5, 1, 2 C in the potential range of 2.6−1.7 V and at a current rate of 5 C in the potential range of 2.6−1.4 V *versus* Li^+/Li at room temperature (where 1 C = 1673 mA g^{-1}). Figure 4b shows the typical discharge−charge voltage profiles of the batteries, showing the highest discharge capacities achieved at different current rates. The discharge profiles for all the current densities were characterized by the two-plateau behavior of a typical sulfur cathode, corresponding to the formation of long-chain polysulfides at 2.3 V and short-chain Li_2S_2 and Li_2S at 2.1 V.[41] No obvious plateau in the charge profiles represent the backward reaction from Li_2S_2/Li_2S to polysulfides, but no complete reverse reaction to sulfur, which is in agreement with CV measurement, shown in Figure 4a.[14] Moreover, the plateaus are very flat with a relatively low polarization at low current rates, which suggests a kinetically efficient reaction process with a small barrier.[15] In addition, the polarization at high current rates is high, which may be due to the small addition amount of electrolyte and the dissolved polysulfides increasing the viscosity of the electrolyte (Experiment Section).[42] The rate capability behavior at different rates is shown in Figure 4c. At 0.25 C, a capacity of 1000 mAh g^{-1} at the first discharge process can be obtained, whereas at higher discharge rates of 0.5, 1, 2, and 5 C, the electrode delivered capacities of 853, 750, 696, and 583 mAh g^{-1}, respectively, demonstrating an excellent rate performance. The high rate performance of the L-GPCS-68% cathode is attributed to the highly dispersed amorphous state sulfur with high electrochemical activity, high electronic conductivity of L-GPC matrix to facilitate electron transport in cathode, and the thin layer of mesoporous carbon with short Li^+ diffusion distances and rapid ion transport. Moreover, the L-GPCS-68%

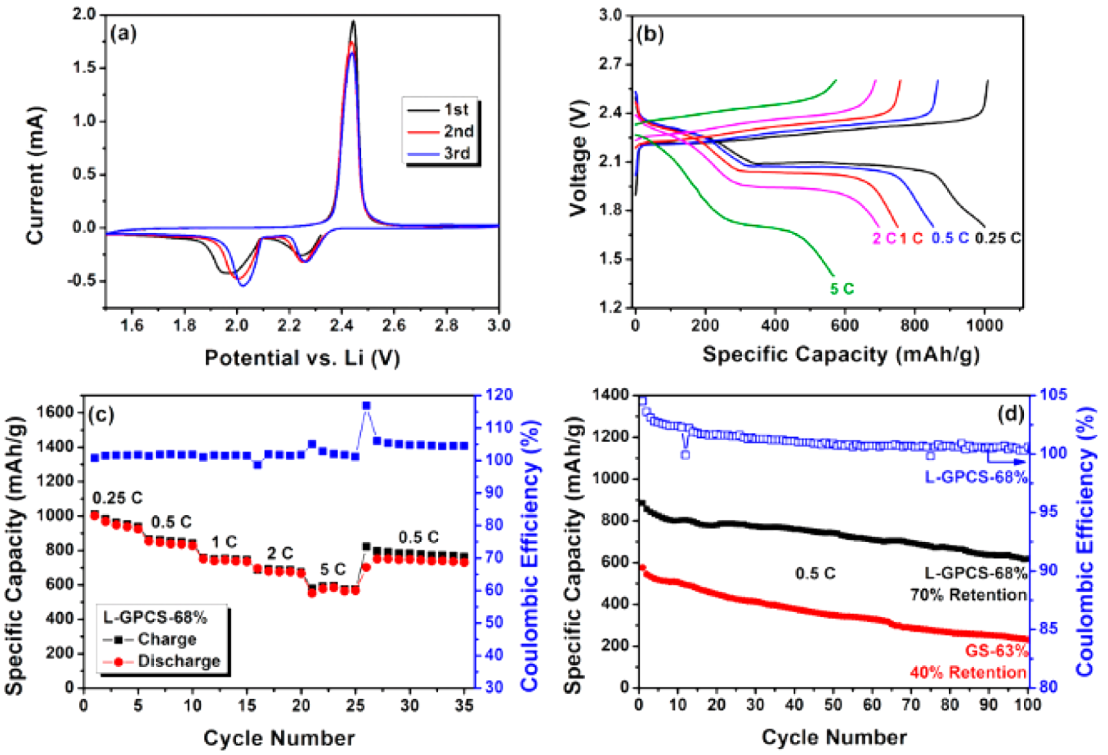

Figure 4. Electrochemical characterization of L-GPCS-68% material as the cathode of Li−S battery. (a) Cyclic voltammetry (CV) measured between 1.5 and 3 V at a sweep rate of 0.1 mV s^{-1} for the first, second, and third cycles. (b) Discharge/charge voltage profiles at various rates from 0.25 to 5 C (1 C = 1675 mA g^{-1}). (c) Discharge/charge capacity cycled at various rates from 0.25 to 5 C. (d) Capacity retention of L-GPCS-68% material cycled at 0.5 C, in comparison with GS-63% material. Specific capacity values were all calculated based on the mass of sulfur.

cathode recovered most of the original capacity when the cycling current was restored to 0.5 C, implying the high reversibility of the L-GPCS-68% electrode even after high rate cycling.

To demonstrate the possible structural advantages of the L-GPCS-68%, a graphene/sulfur (GS) composite was also prepared for comparison (Experimental Section). In the GS composite, sulfur uniformly covered on the surfaces of graphene and no bulk sulfur was observed from SEM images, as shown in Figure S3. TGA determined that the sulfur loading in the GS material is ~63 wt % (denote as GS-63%, Figure S4), and the TG curve of GS-63% is similar to that of the pure state sulfur, demonstrating the weak interaction between sulfur and graphene matrix. The XRD pattern of the GS-63% material exhibits some sharp and strong peaks throughout the entire diffraction range, indicating that the sulfur exists in a well-defined crystal structure (Figure S5).

The cycling performance of the GS-63% and the L-GPCS-68% cathodes are presented in Figure 4d. The GS-63% cathode exhibits an initial discharge capacity of 576.2 mAh g^{-1} with a low sulfur mass loading of 0.18 mg cm^{-2}, and 276 mAh g^{-1} with a high sulfur mass loading of 0.78 mg cm^{-2}, at a current density of 0.5 C (Figure S6), whereas the L-GPCS-68% cathode shows a very high initial discharge capacity of 885.5 mAh g^{-1} with a high sulfur mass loading of 0.74 mg cm^{-2} at the same current density. The GS-63% composite exhibits inferior capacity compared to the L-GPCS-68% composite, indicating the poor utilization of the active sulfur material in GS-63%, due to the poor dispersion and poor electrochemical contact of sulfur. Furthermore, the L-GPCS-68% composite exhibited more stable cycling performance compared with GS-63% composite. After 100 cycles at a current density of 0.5 C, L-GPCS-68% cathode has high capacity retention of ~70%, while GS-63% cathode only has a capacity retention of 40%, representing better cycle stability of L-GPCS-68% composite. The excellent cycle stability of the L-GPCS-68% cathode can be attributed to the pores in the thin layer of porous carbon, which can act as polysulfide reservoirs and prevent polysulfides from diffusing out of the cathode, and diminish the shuttle effect and significantly improve the cycling stability.

To further understanding of the electrochemical performance of GS-63% and L-GPCS-68% composites, electrochemical impedance spectroscopy (EIS) was employed to characterize the fresh batteries. Nyquist plots are shown in Figure 5a; two depressed semicircles are present at high and medium frequency ranges. The depressed semicircle in the high-frequency (HF) region could reflect the charge transfer process at the carbon matrix interface, which dominates the reduction reaction during upper voltage plateau, whereas

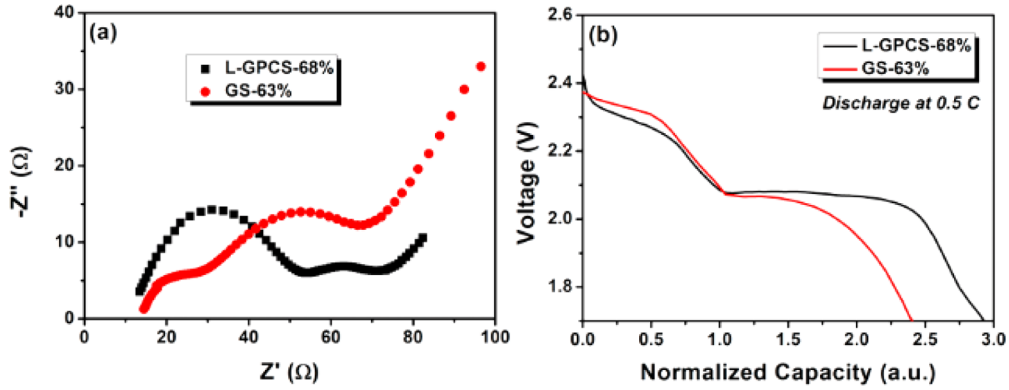

Figure 5. (a) Nyquist plots of GS-63% and L-GPCS-68% cathodes in the frequency range of 100 mHz to 100 kHz. (b) The normalized discharge curves of GS-63% and L-GPCS-68% cathodes at a current density of 0.5 C.

the depressed semicircle in the middle-frequency (MF) range could be attributed to the formation of insoluble polysulfide species, which dominates the lower voltage plateau.[23,43,44] In addition, the intercepts in the high-frequency regions are attributed to the electronic resistance of the cathodes and ionic resistance of the liquid electrolyte, the inclined lines in the low-frequency regions are attributed to the Li^+ transport in cathodes. As shown in Figure 5a, the GS-63% cathode reveals smaller HF semicircle, indicating the faster reaction kinetics of long-chain polysulfides during upper voltage plateau, which is due to the larger addition amount of electrolyte and smaller polysulfides concentration (sulfur/electrolyte mass ratio of GS-63% battery is 1/30, while sulfur/electrolyte mass ratio of L-GPCS-68% battery is 1/10, Figure S7).[42] In contrast, the L-GPCS-68% cathode shows much smaller MF semicircle, indicating the lower polarization and more uniformly deposition of insoluble polysulfide species during lower voltage plateau, which is due to the sulfur in L-GPCS-68% composite with more highly dispersed and more excellent electrochemical contact. These conclusion are consistent with the normalized discharge curves of GS-63% and L-GPCS-68% cathodes, shown in Figure 5b.

CONCLUSION

We have designed and prepared a layered porous carbon−sulfur composite consisting of a graphene layer with thin layers of porous carbon uniformly covering both surfaces. Sulfur is dispersed in this porous carbon. When evaluated as the cathode material of a Li−S battery, the battery displays outstanding electrochemical performance and cycle stability compared with those of a GS composite, which can be attributed to (1) graphene in the composite acts as electronic conductive channel to ensure rapid charge transfer in the composite and the cathode; (2) the porous carbon, covering the graphene with a high surface area and high pore volume, causes the high sulfur content to exist in a highly dispersed amorphous state to improve the conductivity and electrochemical activity; (3) the pores of the porous carbon act as polysulfide reservoirs and confine the polysulfides in the cathode, which can significantly improve the cycling stability.

EXPERIMENTAL SECTION

Synthesis of the Layered Graphene/Porous Carbon−Sulfur (L-GPCS) Composite Material. *L-GPC.* A total of 0.3 g of GO was homogeneously dispersed in 70 mL of H_2O by ultrasonication, then 2.0 g of phenol and 2.9 g of formaldehyde (35 wt %) were added to the GO solution. After stirring for 30 min, the homogeneous dispersion was transferred to a sealed 100 mL Teflon-lined autoclave, heated to 180 °C, and maintained at that temperature for 12 h. The resulting hydrochar was then washed with distilled water and finally dried in vacuum at 120 °C for 24 h. It was then mixed with 4× weight of KOH, and heated at 5 °C min^{-1} to 900 °C for 1 h under Ar. The KOH activated product was thoroughly washed with 0.1 M HCl and distilled water until the pH value reached 7 and finally dried in vacuum at 120 °C for 24 h.

L-GPCS. The L-GPC was added to an appropriate amount of sulfur/CS_2 solution (10 wt % sulfur) and the mixture was stirred at room temperature. Subsequently, the CS_2 was allowed to completely evaporate while stirring. The obtained powder was heated at 160 °C for 12 h in a sealed vessel filled with argon gas to obtain the L-GPCS. The sulfur mass fraction was calculated based on the pore volume of L-GPC to allow for expansion of the pore content upon full lithiation of sulfur to Li_2S.

Synthesis of Graphene/Sulfur (GS) Composite Material. GO (200 mg) was homogeneously dispersed in 60 mL of H_2O by ultrasonication. $Na_2S·9H_2O$ (800 mg) was dissolved in 50 mL of distilled water to form a Na_2S solution, then elemental S (400 mg) was suspended in the Na_2S solution and stirred for 2 h at 60 °C. After dissolution of the sulfur, a sodium polysulfide (Na_2S_x) solution was obtained. Then, the Na_2S_x solution was added to the above-prepared GO dispersions in the presence of 5 wt % surfactant cetyltrimethylammonium bromide (CTAB), and the GO/Na_2S_x blended solution was sonicated for another 2 h and then titrated into 2 mol L^{-1} HCOOH solution until the pH value was less than 5 and stirred for another 2 h. The dispersed suspension was transferred to a sealed 100 mL Teflon-lined autoclave, heated to 180 °C, and held there for 12 h. The resulting solid product was washed with H_2O and finally dried in vacuum at 60 °C for 24 h.

Characterization. The morphologies were analyzed by scanning electron microscopy (SEM) and transmission electron

microscopy (TEM). The SEM was performed on a LEO 1530 VP field emission scanning electron microscope with acceleration voltage of 10 kV. The TEM was carried on Philips T20ST electron microscope at acceleration voltage of 200 kV. Scanning transmission electron microscope (STEM) was carried on a Tecnai G2 F20 electron microscope at an acceleration voltage of 200 kV. Powder X-ray diffraction (XRD) measurements were performed on a Rigaku D/Max-2500 diffractometer with Cu Kα radiation. Thermogravimetric analysis (TGA) was carried out for thermal stability measurements using a NETZSCH STA-409PC instrument. Raman spectra were examined with a LabRAM HRRaman spectrometer using laser excitation at 514.5 nm. The nitrogen adsorption/desorption analysis was done at 77 K on a Micromeritics ASAP 2020 apparatus.

Electrochemical Measurements. To prepare the cathode, 90 wt % of active material was mixed with 10 wt % PVDF binder in NMP to form a slurry. This slurry was then coated onto a carbon-coated aluminum foil using a doctor blade and dried at 50 °C under vacuum to form the cathode. 2032-type coin cells were assembled in an argon-filled glovebox using lithium foil as the counter electrode. The electrolyte used was lithium bis-(trifluoromethanesulfonyl)imide (1 M) in 1:1 (v/v) 1,2-dimethoxy ethane and 1,3-DOL, containing $LiNO_3$ (2 wt %). The mass ratio of sulfur and electrolyte of L-GPCS-68 cathode is fixed at 1/10, and GS-63% cathode is fixed at 1/30 (Figure S7). Specific capacity values were calculated based on the mass of sulfur in the composites. The sulfur content was found to be 68 wt % in L-GPCS, accounting for 62 wt % of the cathode, with a typical sulfur mass loading of 0.65−0.75 mg cm^{-2} and to be 63 wt % in GS, accounting for 57 wt % of the cathode.

Conflict of Interest: The authors declare no competing financial interest.

Acknowledgment. The authors gratefully acknowledge the financial support from MoST (2012CB933401 and 2014CB643502), NSFC (21374050, 51273093 and 51373078), PCSIRT (IRT1257) and Tianjin city (13RCGFGX01121).

Supporting Information Available: The detail characterizations of the layered graphene/porous carbon−sulfur composite and graphene/sulfur composite. This material is available free of charge *via* the Internet at http://pubs.acs.org.

REFERENCES AND NOTES

1. Bruce, P. G.; Freunberger, S. A.; Hardwick, L. J.; Tarascon, J. M. Li-O_2 and Li-S Batteries with High Energy Storage. *Nat. Mater.* **2012**, *11*, 19–29.
2. Tarascon, J. M.; Armand, M. Issues and Challenges Facing Rechargeable Lithium Batteries. *Nature* **2001**, *414*, 359–367.
3. Whittingham, M. S. Lithium Batteries and Cathode Materials. *Chem. Rev.* **2004**, *104*, 4271–4302.
4. Chu, M. Y. Rechargeable Positive Electrodes. U.S. Patent US5686201A, 1997.
5. Ji, X.; Lee, K. T.; Nazar, L. F. A Highly Ordered Nanostructured Carbon-Sulphur Cathode for Lithium-Sulphur Batteries. *Nat. Mater.* **2009**, *8*, 500–506.
6. Jayaprakash, N.; Shen, J.; Moganty, S. S.; Corona, A.; Archer, L. A. Porous Hollow Carbon@Sulfur Composites for High-Power Lithium-Sulfur Batteries. *Angew. Chem., Int. Ed.* **2011**, *50*, 5904–5908.
7. Guo, J.; Xu, Y.; Wang, C. Sulfur-Impregnated Disordered Carbon Nanotubes Cathode for Lithium-Sulfur Batteries. *Nano Lett.* **2011**, *11*, 4288–4294.
8. Chen, H.; Dong, W.; Ge, J.; Wang, C.; Wu, X.; Lu, W.; Chen, L. Ultrafine Sulfur Nanoparticles in Conducting Polymer Shell as Cathode Materials for High Performance Lithium/Sulfur Batteries. *Sci. Rep.* **2013**, *3*, 1910.
9. Xin, S.; Gu, L.; Zhao, N. H.; Yin, Y. X.; Zhou, L. J.; Guo, Y. G.; Wan, L. J. Smaller Sulfur Molecules Promise Better Lithium-Sulfur Batteries. *J. Am. Chem. Soc.* **2012**, *134*, 18510–18513.
10. Suo, L.; Hu, Y. S.; Li, H.; Armand, M.; Chen, L. A New Class of Solvent-In-Salt Electrolyte for High-Energy Rechargeable Metallic Lithium Batteries. *Nat. Commun.* **2013**, *4*, 1481.
11. Fu, Y.; Su, Y. S.; Manthiram, A. Highly Reversible Lithium/Dissolved Polysulfide Batteries with Carbon Nanotube Electrodes. *Angew. Chem., Int. Ed.* **2013**, *52*, 6930–6935.
12. Su, Y. S.; Manthiram, A. Lithium-Sulphur Batteries with a Microporous Carbon Paper as a Bifunctional Interlayer. *Nat. Commun.* **2012**, *3*, 1166.
13. Seh, W. Z.; Li, W.; Cha, J. J.; Zheng, G.; Yang, Y.; McDowell, M. T.; Hsu, P. C.; Cui, Y. Sulphur-TiO_2 Yolk-Shell Nanoarchitecture with Internal Void Space for Long-Cycle Lithium-Sulphur Batteries. *Nat. Commun.* **2013**, *4*, 1331.
14. Zheng, G.; Yang, Y.; Cha, J. J.; Hong, S. S.; Cui, Y. Hollow Carbon Nanofiber-Encapsulated Sulfur Cathodes for High Specific Capacity Rechargeable Lithium Batteries. *Nano Lett.* **2011**, *11*, 4462–4467.
15. Zhou, G.; Pei, S.; Li, L.; Wang, D. W.; Wang, S.; Huang, K.; Yin, L. C.; Li, F.; Cheng, H. M. A Graphene-Pure-Sulfur Sandwich Structure for Ultrafast, Long-Life Lithium-Sulfur Batteries. *Adv. Mater.* **2013**, *26*, 625–631.
16. Ji, L.; Rao, M.; Zheng, H.; Zhang, L.; Li, Y.; Duan, W.; Guo, J.; Cairns, E. J.; Zhang, Y. Graphene Oxide as a Sulfur Immobilizer in High Performance Lithium/Sulfur Cells. *J. Am. Chem. Soc.* **2011**, *133*, 18522–18525.
17. Mikhaylik, Y. V.; Akridge, J. R. Polysulfide Shuttle Study in the Li/S Battery System. *J. Electrochem. Soc.* **2004**, *151*, A1969–A1976.
18. Li, X.; Cao, Y.; Qi, W.; Saraf, L. V.; Xiao, J.; Nie, Z.; Mietek, J.; Zhang, J. G.; Schwenzer, B.; Liu, J. Optimization of Mesoporous Carbon Structures for Lithium-Sulfur Battery Applications. *J. Mater. Chem.* **2011**, *21*, 16603–16610.
19. Elazari, R.; Salitra, G.; Garsuch, A.; Panchenko, A.; Aurbach, D. Sulfur-Impregnated Activated Carbon Fiber Cloth as a Binder-Free Cathode for Rechargeable Li-S Batteries. *Adv. Mater.* **2011**, *23*, 5641–5644.
20. Liang, C.; Dudney, N. J.; Howe, J. Y. Hierarchically Structured Sulfur/Carbon Nanocomposite Material for High-Energy Lithium Battery. *Chem. Mater.* **2009**, *21*, 4724–4730.
21. Li, W.; Zhang, Q.; Zheng, G.; Seh, Z. W.; Yao, H.; Cui, Y. Understanding the Role of Different Conductive Polymers in Improving the Nanostructured Sulfur Cathode Performance. *Nano Lett.* **2013**, *13*, 5534–5540.
22. Zhou, W.; Yu, Y.; Chen, H.; DiSalvo, F. J.; Abruna, H. C. D. Yolk-Shell Structure of Polyaniline-Coated Sulfur for Lithium-Sulfur Batteries. *J. Am. Chem. Soc.* **2013**, *135*, 16736–16743.
23. Li, W.; Zheng, G.; Yang, Y.; Seh, Z. W.; Liu, N.; Cui, Y. High-Performance Hollow Sulfur Nanostructured Battery Cathode through a Scalable, Room Temperature, One-Step, Bottom-Up Approach. *Proc. Natl. Acad. Sci. U.S.A.* **2013**, *110*, 7148–7153.
24. Li, G. C.; Li, G. R.; Ye, S. H.; Gao, X. P. A Polyaniline-Coated Sulfur/Carbon Composite with an Enhanced High-Rate Capability as a Cathode Material for Lithium/Sulfur Batteries. *Adv. Energy Mater.* **2012**, *2*, 1238–1245.
25. Zheng, G.; Zhang, Q.; Cha, J. J.; Yang, Y.; Li, W.; Seh, Z. W.; Cui, Y. Amphiphilic Surface Modification of Hollow Carbon Nanofibers for Improved Cycle Life of Lithium Sulfur Batteries. *Nano Lett.* **2013**, *13*, 1265–1270.
26. Zhou, G.; Yin, L. C.; Wang, D. W.; Li, L.; Pei, S.; Gentle, I. R.; Li, F.; Cheng, H. M. Fibrous Hybrid of Graphene and Sulfur Nanocrystals for High-Performance Lithium-Sulfur Batteries. *ACS Nano* **2013**, *7*, 5367–5375.
27. Evers, S.; Nazar, L. F. Graphene-Enveloped Sulfur in A One Pot Reaction: A Cathode with Good Coulombic Efficiency and High Practical Sulfur Content. *Chem. Commun.* **2012**, *48*, 1233–1235.
28. Wang, H.; Yang, Y.; Liang, Y.; Robinson, J. T.; Li, Y.; Jackson, A.; Cui, Y.; Dai, H. Graphene-Wrapped Sulfur Particles as a Rechargeable Lithium-Sulfur Battery Cathode Material with High Capacity and Cycling Stability. *Nano Lett.* **2011**, *11*, 2644–2647.
29. Zu, C.; Manthiram, A. Hydroxylated Graphene-Sulfur Nanocomposites for High-Rate Lithium-Sulfur Batteries. *Adv. Energy Mater.* **2013**, *3*, 1008–1012.
30. Lin, T.; Tang, Y.; Wang, Y.; Bi, H.; Liu, Z.; Huang, F.; Xie, X.; Jiang, M. Scotch-Tape-Like Exfoliation of Graphite Assisted

with Elemental Sulfur and Graphene-Sulfur Composites for High-Performance Lithium-Sulfur Batteries. *Energy Environ. Sci.* **2013**, *6*, 1283–1290.
31. Huang, J. Q.; Liu, X. F.; Zhang, Q.; Chen, C. M.; Zhao, M. Q.; Zhang, S. M.; Zhu, W.; Qian, W. Z.; Wei, F. Entrapment of Sulfur in Hierarchical Porous Graphene for Lithium-Sulfur Batteries with High Rate Performance from −40 to 60 °C. *Nano Energy* **2013**, *2*, 314–321.
32. Cao, Y.; Li, X.; Aksay, I. A.; Lemmon, J.; Nie, Z.; Yang, Z.; Liu, J. Sandwich-Type Functionalized Graphene Sheet-Sulfur Nanocomposite for Rechargeable Lithium Batteries. *Phys. Chem. Chem. Phys.* **2011**, *13*, 7660–7665.
33. Wang, L.; Wang, D.; Zhang, F.; Jin, J. Interface Chemistry Guided Long-Cycle-Life Li-S Battery. *Nano Lett.* **2013**, *13*, 4206–4211.
34. Zhou, W.; Chen, H.; Yu, Y.; Wang, D.; Cui, Z.; DiSalvo, F. J.; Abruna, H. D. Amylopectin Wrapped Graphene Oxide/Sulfur for Improved Cyclability of Lithium-Sulfur Battery. *ACS Nano* **2013**, *7*, 8801–8808.
35. Zhang, L.; Zhang, F.; Yang, X.; Long, G.; Wu, Y.; Zhang, T.; Leng, K.; Huang, Y.; Ma, Y.; Yu, A.; Chen, Y. Porous 3D Graphene-Based Bulk Materials with Exceptional High Surface Area and Excellent Conductivity for Supercapacitors. *Sci. Rep.* **2013**, *3*, 1408.
36. Biener, J.; Dasgupta, S.; Shao, L.; Wang, D.; Worsley, M. A.; Wittstock, A.; Lee, J. R. I.; Biener, M. M.; Orme, C. A.; Kucheyev, S. O.; *et al.* Macroscopic 3D Nanographene with Dynamically Tunable Bulk Properties. *Adv. Mater.* **2012**, *24*, 5083–5087.
37. Shinkarev, V. V.; Fenelonov, V. B.; Kuvshinov, G. G. Sulfur Distribution on the Surface of Mesoporous Nanofibrous Carbon. *Carbon* **2003**, *41*, 295–302.
38. Pimenta, M. A.; Dresselhaus, G.; Dresselhaus, M. S.; Cancado, L. G.; Jorio, A.; Saito, R. Studying Disorder in Graphite-Based Systems by Raman Spectroscopy. *Phys. Chem. Chem. Phys.* **2007**, *9*, 1276–1290.
39. Zhang, S. S. Role of $LiNO_3$ in Rechargeable Lithium/Sulfur Battery. *Electrochim. Acta* **2012**, *70*, 344–348.
40. Zhang, S. S. Liquid Electrolyte Lithium/Sulfur Battery: Fundamental Chemistry, Problems, and Solutions. *J. Power Sources* **2013**, *231*, 153–162.
41. Yin, Y. X.; Xin, S.; Guo, Y. G.; Wan, L. J. Lithium-Sulfur Batteries: Electrochemistry, Materials, and Prospects. *Angew. Chem., Int. Ed.* **2013**, *52*, 13186–13200.
42. Zhang, S. S. Improved Cyclability of Liquid Electrolyte Lithium/Sulfur Batteries by Optimizing Electrolyte/Sulfur Ratio. *Energies* **2012**, *5*, 5190–5197.
43. Barchasz, C.; Lepretre, J. C.; Alloin, F.; Patoux, S. New Insights into the Limiting Parameters of the Li/S Rechargeable Cell. *J. Power Sources* **2012**, *199*, 322–330.
44. Yuan, L.; Qiu, X.; Chen, L.; Zhu, W. New Insight into the Discharge Process of Sulfur Cathode by Electrochemical Impedance Spectroscopy. *J. Power Sources* **2009**, *189*, 127–132.